Received: 13 March 2020 | Revised: 11 June 2020 | Accepted: 20 June 2020

DOI: 10.1002/jccs.202000106

JOURNAL OF THE CHINESE CHEMICAL SOCIETY

SPECIAL ISSUE PAPER

Weak interactions in imidazole-containing zinc(II)-based metal–organic frameworks

Hsin-Wei Wu[1,2] | **Li-Wei Lee**[1] | **Pounraj Thanasekaran**[3] | **Cing-Huei Su**[3] | **Yen-Hsiang Liu**[3] | **Tsung-Mei Chin**[2] | **Kuang-Lieh Lu**[1,3]

[1]Institute of Chemistry, Academia Sinica, Taipei, Taiwan

[2]Department of Chemistry, Chinese Culture University, Taipei, Taiwan

[3]Department of Chemistry, Fu Jen Catholic University, New Taipei City, Taiwan

Correspondence
Kuang-Lieh Lu, Institute of Chemistry, Academia Sinica, Taipei 115, Taiwan.
Email: kllu@gate.sinica.edu.tw

Yen-Hsiang Liu, Department of Chemistry, Fu Jen Catholic University, New Taipei City 242, Taiwan.
Email: chemyhl@gmail.com

Tsung-Mei Chin, Department of Chemistry, Chinese Culture University, Taipei 111, Taiwan.
Email: tmchin@faculty.pccu.edu.tw

Funding information
Ministry of Science and Technology, Taiwan, Grant/Award Number: MOST-106-2113-M-001-032; Academia Sinica

Abstract

The self-assembly of the two zinc(II) metal–organic frameworks, $[Zn_2(L)(bdc)_2]\cdot 3MeOH\cdot 4H_2O\}_n$ (**1**, L = 2-(pyridin-4-yl)-3H-imidazo[4,5-c]pyridine, H_2bdc = 1,4-benzenedicarboxylic acid) and $[Zn_2(L)(bdc)_2]\cdot 2DMF\cdot H_2O\}_n$ (**2**), was achieved under mild reaction conditions. Both compounds **1** and **2** were structurally characterized by single-crystal X-ray diffraction analysis. Interestingly, the coordination modes of the ligand L in two structures are entirely different. Compounds **1** and **2** were made up of paddle wheel-shaped $\{Zn_2(O_2C)_4\}$ secondary building unit (SBU) clusters, which adopted three-dimensional structures with a *pcu* topology. Rich weak interactions were observed in the structures of both **1** and **2**. The uncoordinated imidazole and pyridine moieties exhibited electron donor–acceptor interactions, π–π stacking, hydrogen bonding, and CH–π interactions. These interactions also facilitated the abilities of the framework to adsorb CO_2 molecules. Gas adsorption studies revealed that compound **1** selectively adsorbed CO_2 (131.1 cm^3/g) over N_2 (23.5 cm^3/g) and H_2 (36.5 cm^3/g) at a pressure of 1 atm.

KEYWORDS

coordination mode, metal–organic frameworks, structure, weak interactions, zinc

1 | INTRODUCTION

It is well known that metal–organic frameworks (MOFs) have a number of unique features, which make them extraordinarily applicable for use in a variety of fields.[1–13] Among those features, rich weak interactions in MOFs are highly significant in terms of tuning the orientations of the building units, stabilizing the overall structures, influencing the functionalities, and the potential applications of these materials. Interestingly, the design of a multifunctional ligand containing imidazole moieties can be used not only to fabricate MOFs with unique network topologies but can also be utilized to alter their properties while still maintaining their porosity.[14–16] This type of ligand is also an excellent model for examining weak interactions in MOFs due to their intrinsic hydrogen bonding and π–π stacking interactions. In addition, weak interactions of MOFs with small molecules such as H_2, CH_4, and CO_2 have also attracted interest as these MOF–guest interactions facilitate their gas adsorption–desorption and sensing capacities.[17–24] Although the synthesis and properties of a number of imidazole-containing MOFs have been reported,[14–16,25–29] the integration of an imidazole group with two pyridine moieties in a coordinated ligand in an MOF has rarely been addressed.[30–33]

Here, we report on the selection of a model ligand L (L = 2-(pyridin-4-yl)-3H-imidazo[4,5-c]pyridine), from which two MOFs, $[Zn_2(L)(bdc)_2]\cdot 3MeOH\cdot 4H_2O\}_n$ (**1**, H_2bdc = 1,4-benzenedicarboxylic acid) and $[Zn_2(L)(bdc)_2]\cdot 2DMF\cdot H_2O\}_n$ (**2**) (Scheme 1), were synthesized. Interestingly, the coordination modes of the ligand L in the two products are completely different in each structure. The multiple N-donor sites of the L ligand play important roles in enhancing electron donor–acceptor interactions, π–π stacking, and hydrogen bonding interactions. These interactions allow compound **1** to display a high adsorption capacity and good selectivity for CO_2 (131.1 cm^3/g) over N_2 (23.5 cm^3/g) and H_2 (36.5 cm^3/g) at a pressure of 1 atm.

2 | RESULTS AND DISCUSSION

Compounds **1** and **2** were self-assembled from the reaction of $Zn(NO_3)_2\cdot 6H_2O$, 2-(pyridin-4-yl)-3H-imidazo[4,5-c]pyridine (L) and 1,4-benzenedicarboxylic acid (H_2bdc) in a H_2O/MeOH/DMF solution (using THF buffer for **2** only) under mild reaction conditions (Scheme 1).

2.1 | Structural description of $\{[Zn_2(L)(bdc)_2]\cdot 3MeOH\cdot 4H_2O\}_n$ (1)

A single-crystal X-ray diffraction analysis revealed that compound **1** crystallizes in a monoclinic unit cell with space group $P2_1/c$. The crystallographic asymmetric unit contains two zinc(II) cations, two bdc^{2-} ligands, one L ligand, and disordered guest methanol, as well as water molecules. Due to the disordered nature, only one of the methanol molecules was located from the electron density map. The assignment of the guest molecules was further investigated by thermogravimetric measurements. Two zinc ions are coordinated by four carboxylate groups from the bdc^{2-} ligands to form a $Zn_2(O_2C)_4$ paddle wheel-shaped secondary building unit (SBU). In addition, these two zinc ions in the paddle wheel-shaped SBU are further bound by the pyridine moieties from two separated L ligands, leading to a 6-connecting node (Figure 1a, Scheme 2). As a result, compound **1** presents a three-dimensional (3D) framework with a *pcu* topology (Figure 1b). Due to the large cavity space of the resulting *pcu*-type 3D-net, a twofold intepenetration of the 3D network was observed in **1** (Figure 1c). It is worth noting that a net-to-net π–π interaction is observed, which serves to enhance the stability of the interpenetrated network (Figure 1d). In spite of the interpenetration behavior, a PLATON analysis of the potential solvent accessible area indicated that extra-framework spaces (38.9% of the unit cell volume) are available for the potential inclusion of guest molecules. It is also worth noting that the imidazole ring of the bridging L ligand provides multiple N-sites (Scheme 2, Type I) that are available for hydrogen bonding interactions, as well as electron donor–acceptor interactions (Figure 1e). The imidazole ring carries dual Bronsted and Lewis acid-base interactions.

2.2 | Structural description of $\{[Zn_2(L)(bdc)_2]\cdot 2DMF\cdot H_2O\}_n$ (2)

A single-crystal X-ray diffraction analysis revealed that compound **2** crystallizes in a monoclinic unit cell with space group $C2/c$. The crystallographic asymmetric unit contains a zinc (II) cation, one bdc^{2-} ligand, half of an L ligand, and a guest DMF molecule, as well as disordered water molecules. Because of the disordered nature of the guest molecules, only the DMF molecule was located on the electron density map. The assignment of the disordered guest water molecules was further examined by thermogravimetric measurements. Similar to compound **1**, two zinc ions are coordinated by four carboxylate groups from the bdc^{2-} ligands to form a $Zn_2(O_2C)_4$ paddle wheel-shaped SBU. Two L ligands are coordinated to the zinc centers through the axial position of the paddle wheel-shaped SBU, leading to a 6-connecting node and a three-dimensional framework with a *pcu* topology (Figure 2). Unlike compound **1**, the imidazole N-sites of the L ligand participate in the coordination with zinc centers instead of pyridyl groups (Scheme 2, Type II). Due to the short length of the linkages, self-interpenetration behavior was not observed for compound **2**. The PLATON analysis of the potential solvent accessible area indicated that there are extra-framework spaces (51.4% of the unit cell

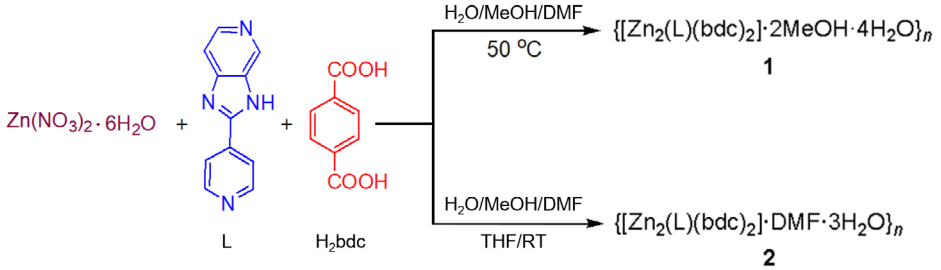

SCHEME 1 Route for the preparation of compounds **1** and **2**

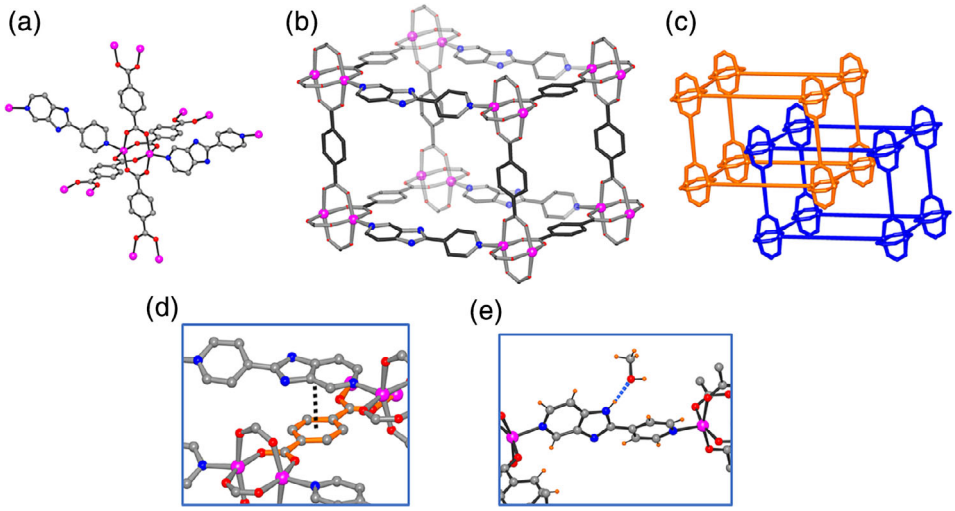

FIGURE 1 Crystal structure of compound **1**. (a) paddle wheel-shaped structure of the zinc ion coordinated with the bdc^{2-} ligand, (b) three-dimensional structure of the zinc ion coordinated with the bdc^{2-} and the L ligand, (c) twofold interpenetration of the 3D network, (d) net-to-net π–π interaction in the interpenetrated network, and (e) hydrogen bonding interactions and electron donor–acceptor interactions

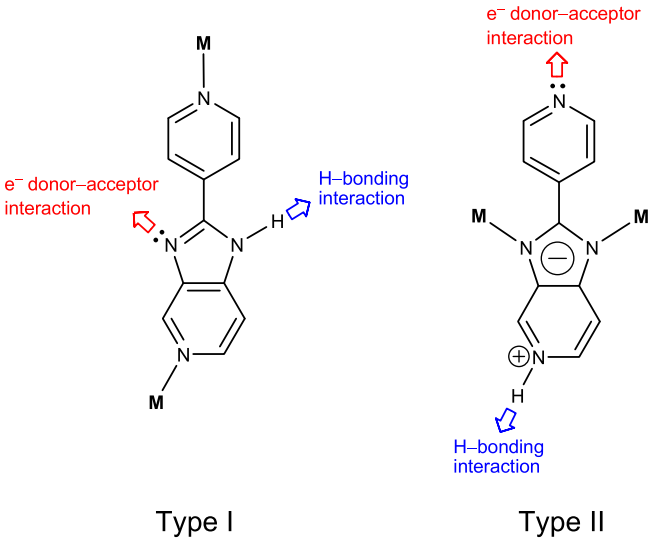

SCHEME 2 Multiple N-donor sites of the ligand L. Type I is observed in compound **1**, whereas Type II appears in compound **2**

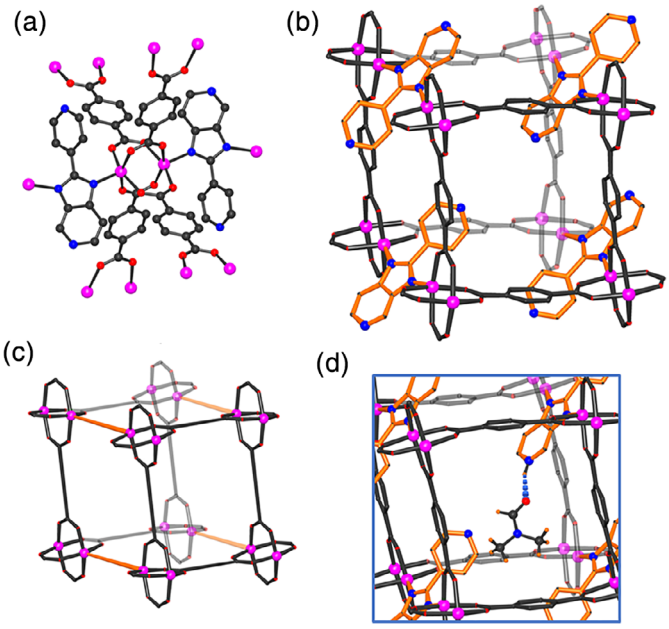

FIGURE 2 Crystal structure of compound **2**. (a) Paddle wheel-shaped 6-connecting node of **2**, (b) perspective view of the 3D network of **2**, (c) topological view of the network of **2**, and (d) graphical representation of the uncoordinated N-site of the pyridyl ring engaging electron donor–acceptor and hydrogen bonding interactions

volume), which are potentially available for the inclusion of guest molecules. Although the coordination mode of the bridging ligand L in compound **2** is different from that in **1** (Scheme 2), the uncoordinated pyridyl ring in **2** is also available for hydrogen bonding interactions, as well as electron donor–acceptor interactions (Figure 2d).

2.3 | Comparison of the structures in compounds 1 and 2

It would be interesting to compare the structures of compounds **1** and **2** because the coordination modes of L are entirely different. The ligand L contains multiple N-donor sites. As shown in Scheme 1, a type I coordination mode is observed in compound **1**, where the long-end N-donor sites from two separated pyridines provide the long linkage that connects the two paddle wheel units. This type of coordination creates a large void in the cubic unit of a *pcu* net, leading to the formation of a twofold interpenetrated 3D network. Extensive net-to-net π–π interactions in the interpenetrated network are observed, which function to stablize the interpenetrated structure of **1**. In addition, hydrogen bonding and electron donor–acceptor

interactions between methanol guest molecules and the uncoordinated imidazole moiety are apparent.

It is particularly interesting that the type II coordination mode of the L ligand appears in compound **2**. In this case, the side-on linkage through the imidazole moiety of the L ligand is bonded to two metal centers, as shown in Scheme 1. To the best of our knowledge, this constitutes the first report of this type of coordination mode. The length through the side-on imidazole linkages appeared to be too short so that self-interpenetration of the network does not occur. This finally creates a large extra-framework space in the resulting *pcu* net of **2**, which can accommodate large guest molecules, such as DMF. Although π–π stacking interactions are not observed in the structure of **2**, electron donor–acceptor and hydrogen bonding interactions between the uncoordinated N-site of the pyridyl ring and the DMF molecule are evident (Figure 2d).

2.4 | Thermogravimetric and PXRD analyses

Thermogravimetric analyses (TGA) analyses were performed for compounds **1** and **2** in an attempt to access the thermal stability and structural variation as a function of temperature. The thermogravimetric analysis of **1** showed that solvent molecules are eliminated from the network (calcd 16.2%, found 16.1%), which corresponds to the loss of H_2O and MeOH guest molecules when the temperature is increased from room temperature to about 160°C (Figure S5). Regarding compound **2**, after the loss of the guest H_2O and DMF molecules (calcd 15.8%, found 15.8%) at a temperature of about 100–200°C, the structure was maintained until the temperature reached 300°C, after which, it began to decompose (Figure S5). The experimentally obtained PXRD patterns for compounds **1** and **2** were consistent with the simulated patterns calculated from the single-crystal data (Figure S6).

2.5 | Gas adsorption properties and selectivity

Inspired by the microporous features and uncoordinated N-functionalized pores, compound **1** was examined as a candidate for the selective adsorption of gas molecules. Calculations indicated that the porosity of compound **1** was 38.9%. The Brunauer–Emmett–Teller (BET) surface area and Langmuir surface area were determined to be 41.7 and 110.9 m^2/g, respectively. The results of sorption studies revealed that compound **1** exhibited low N_2 and H_2 uptake capacities of 23.5 and 36.5 cm^3/g at 77 K, respectively, at 1 atm with irreversible type II isotherms (Figure S7).[22,34] The CO_2 adsorption of compound **1** at 1 atm and controlled temperature at 195 K showed typical type I isotherm. Measurement of the CO_2 sorption isotherm at 195 K revealed that compound **1** has a relatively higher CO_2 loading of 131.1 cm^3/g, while at 273 and 298 K, the values were 27.5 and 19.4 cm^3/g, respectively (Figure 3). The enhancement of CO_2 uptake for **1** at 195 K can be attributed to the lone pair of electrons in the uncoordinated —N and —NH moieties from the ligand L in the channels that can induce electron donor–acceptor and hydrogen bonding interactions with CO_2 molecules. The value for the uptake of CO_2 for compound **1** is comparable with those of many other well-known Zn(II)- and Cd(II)-based MOFs.[13,23,24,35–42] We therefore propose that the CO_2 is trapped inside the channel of **1** via interactions of the —N and —NH moieties of the ligands with CO_2, leading to the formation of a hysteresis in type I isotherm, thereby preserving CO_2 molecules.

3 | EXPERIMENTAL SECTION

3.1 | Materials and instruments

All chemicals were purchased commercially and were used as received without further purification. Infrared spectra were recorded on a Perkin-Elmer Paragon 1000 FT-IR spectrophotometer in the region 4000–400 cm^{-1}. Powder X-ray diffraction measurements were performed at room temperature using a Siemens D-5000 diffractometer at 40 kV and 30 mA for Cu Kα radiation (λ = 1.5406 Å) with a step size of 0.02° in θ and a scan speed of 1 s per step size. Thermogravimetric analyses were performed in an atmosphere of nitrogen with a Perkin-Elmer TGA-7 TG analyzer. BET analyses were

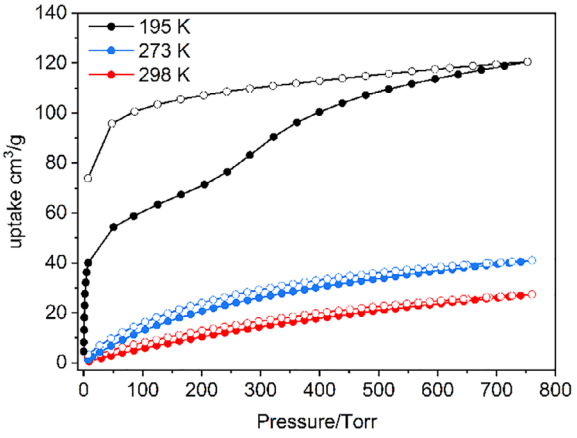

FIGURE 3 Adsorption isotherms of CO_2 of **1** measured at a temperature of 195, 273, and 298 K

investigated with a Micrometrics ASAP 2020 system using nitrogen and hydrogen as the adsorbates at 77 K and carbon dioxide as the adsorbate at 195, 273, and 293 K.

3.2 | Preparation of 2-(pyridin-4-yl)-3H-imidazo[4,5-c]pyridine (L)

The ligand 2-(pyridin-4-yl)-3H-imidazo[4,5-c]pyridine (L) was synthesized as reported previously (Scheme S2).[43] In a typical run, the ligand **L** was prepared by heating a mixture of pyridine-3,4-diamine (1.3 g, 11.9 mmol), isonicotinic acid (1.6 g, 12.9 mmol), and polyphosphoric acid (15 g, 16.0 mmol) at 180°C for 12 hr under a nitrogen atmosphere. The resulting mixture was then cooled to room temperature followed by the addition of 50 ml of H_2O. The pH of the resulting solution was then adjusted to 7 with ammonia, which resulted in the formation of a precipitate. Colorless powdered products were obtained after recrystallization. Yield: 75% (1.8 g, 8.9 mmol). IR (KBr, cm^{-1}): 3240, 1625, 1603, 1579, 1549, 1457, 1438, 1387, 1368, 1243, 817, 766. ^1H NMR (300 MHz, CD_3OD-*d*4, ppm): δ = 7.68 (d, 1H), 8.14 (d, 2H), 8.26 (d,1H), 8.70 (d, 2H), 8.9 (s, 1H).

3.3 | Synthesis of $[Zn_2(L)(bdc)_2]\cdot 3MeOH\cdot 4H_2O\}_n$ (1)

A total of 2 ml of H_2O/MeOH (1:1 vol/vol) mixture of Zn $(NO_3)_2\cdot 6H_2O$ (8.9 mg, 0.03 mmol) and 2-(pyridine-4-y1)-3H-imidazo[4,5-c]pyridine (L, 6.1 mg, 0.03 mmol) was dissolved in 2 ml of a DMF/MeOH (1:1 vol/vol) solution containing 1,4-benzenedicarboxylic acid (H_2bdc, 5.0 mg, 0.03 mmol), sealed in a closed glass tube, and then heated at 50°C for 48 hr in a water bath. Colorless block-shaped crystals of compound **1** were formed in 31% yield (7.3 mg, based on $Zn(NO_3)_2\cdot 6H_2O$). The solid products were isolated on a filter and dried in air. IR (KBr, cm^{-1}): 3392, 3170, 3098, 2864, 2810, 1663, 1637, 1504, 1436, 1293, 1254, 1227, 1176, 1152, 1095, 1066, 1016, 934, 885, 824, 746, 715, 662, 610, 596, 548.

3.4 | Synthesis of $[Zn_2(L)(bdc)_2]\cdot 2DMF\cdot H_2O\}_n$ (2)

Two ml of a H_2O/MeOH (1:1 vol/vol) solution containing $Zn(NO_3)_2\cdot 6H_2O$ (8.8 mg, 0.03 mmol) and 2-(pyridine-4-y1)-3H-imidazo[4,5-c]pyridine (L, 5.9 mg, 0.03 mmol) was dissolved in 2 ml of DMF/MeOH (1:1 vol/vol) solution containing 1,4-benzenedicarboxylic acid (H_2bdc, 5.0 mg, 0.03 mmol), followed by the addition of tetrahydrofuran (THF). The resulting solution was sealed in a closed glass tube, which was then allowed to stand at room temperature for 1 month, whereupon colorless rectangular crystals of compound **2** were formed. The solid products were isolated on a filter and dried in air. IR (KBr, cm^{-1}): 3419, 3098, 2930, 2863, 1957, 1673, 1628, 1502, 1323, 1255, 1173, 1149, 1095, 1063, 1015, 887, 823, 749, 701, 664, 596, 573, 545.

3.5 | Crystallographic measurements

Single crystals of **1** and **2** suitable for X-ray diffraction were placed in a cooled stream of N_2 gas at 200 K and 296 K, respectively, for intensity data collection on a Bruker Kappa CCD diffractometer with graphite monochromated Mo-Kα (λ = 0.71073 Å) radiation. Data reduction included absorption corrections by the MULTISCAN method, using the HKL SCALEPACK[44] and SADABS.[45] Crystal data and experimental details are given in Table 1. The X-ray structure was determined by direct methods and difference Fourier techniques and refined by full-matrix least squares, using the SHELXL97 program.[46] All nonhydrogen atoms were refined anisotropically. The C-bound and N-bound H atoms were placed in the calculated positions and refined by the riding model approximation. Due to the uncertainty in locating the disordered guest molecules, only some of the guest molecules were located from the difference Fourier map in compounds **1** and **2**. The crystallographic data for **1** and **2** were deposited at the Cambridge Crystallographic Data Centre; the deposition numbers for **1** and **2** are CCDC 1990125 and 1990126, respectively.

4 | CONCLUSIONS

In this work, we report on the successful synthesis of two Zn-based MOFs from an imidazole derivative and a dicarboxylate linker under mild reaction conditions. The imidazole moiety exhibits two different coordination modes with respect to the Zn metal centers, leading to the formation of structurally different compounds, that is, **1** and **2**. Although the coordination modes of the imidazole group are very different, rich weak interactions including electron donor–acceptor interactions, π–π stacking, hydrogen bonding, and CH–π interactions occur in the structures. These weak interactions not only dictate the topology and stabilize the final structures but also facilitate the adsorption of gas within the porous MOFs. Compound **1** showed good selectivity for CO_2 over N_2 and H_2 due to hydrogen-bonding interaction as well as

TABLE 1 Crystal data and structure refinement for compounds **1** and **2**

Compound	1	2
Empirical formula	$C_{56}H_{40}N_8O_{18}Zn_4$	$C_{33}H_{29}N_6O_{10}Zn_2$
Formula weight	1,374.44	800.36
Temperature (K)	200 (2)	296 (2)
Wavelength (Å)	0.71073	0.71073
Crystal system	Monoclinic	Monoclinic
Space group	$P2_1/c$	$C2/c$
R_{int}	0.0422	0.0403
a (Å)	10.9546(5)	23.3639(12)
b (Å)	10.9340(4)	14.4683(7)
c (Å)	30.2273(11)	16.1959(8)
β (°)	93.624(2)	128.345(2)
V (Å^3)	3,613.3(2)	4,293.8(4)
Z	2	4
ρ_{calcd} (mg/m^3)	1.263	1.238
Absorption coefficient	1.376 mm^{-1}	1.170 mm^{-1}
F(000)	1,392	1,636
Crystal size (mm)	0.42 × 0.21 × 0.04	0.35 × 0.24 × 0.18
Range for data collection	1.86–25.00°	1.79–25.14°
Limiting indices	−12 < =h < =9,-12 < =k < =12, −35 < =l < =35	−27 < =h < =27, -16 < =k < =17, −19 < =l < =15
Reflections collected	24,510	14,803
Reflections unique	6,308	3,798
Completeness to θ	99.6%	98.7%
Max. and min. Transmission	0.9470 and 0.5958	0.8170 and 0.6849
Data/restraints	6,308/0	3,798/0
No. of parameters	388	219
Goodness-of-fit on F^2	1.038	1.081
Final R indices ($I > 2\sigma(I)$)	R1 = 0.0444 wR2 = 0.1027	R1 = 0.0691 wR2 = 0.1931
R indices (all data)	R1 = 0.0618 wR2 = 0.1078	R1 = 0.0753 wR2 = 0.1984

Note: $R_1 = \Sigma||F_0|-|F_c||/\Sigma|F_0|$; $wR_2 = [\Sigma w(F_0^2-F_c^2)^2/\Sigma w(F_0^2)^2]^{1/2}$.

electron donor–acceptor interaction between the CO_2 and N atoms of the MOF.

ACKNOWLEDGMENTS

We gratefully acknowledge the Academia Sinica and the Ministry of Science and Technology (grant number MOST-106-2113-M-001-032), Taiwan, for the financial support.

ORCID

Kuang-Lieh Lu https://orcid.org/0000-0002-5529-7126

REFERENCES

[1] N. Stock, S. Biswas, *Chem. Rev.* **2012**, *112*, 933.
[2] H. Furukawa, K. E. Cordova, M. O'Keeffe, O. M. Yaghi, *Science* **2013**, *341*, 1230444.
[3] D. Yu, Q. Shao, Q. Song, J. Cui, Y. Zhang, B. Wu, L. Ge, Y. Wang, Y. Zhang, Y. Qin, R. Vajtai, P. M. Ajayan, H. Wang, T. Xu, Y. Wu, *Nat. Commun.* **2020**, *11*, 927.
[4] S. Yuan, L. Feng, K. Wang, J. Pang, M. Bosch, C. Lollar, Y. Sun, J. Qin, X. Yang, P. Zhang, Q. Wang, L. Zou, Y. Zhang, L. Zhang, Y. Fang, J. Li, H.-C. Zhou, *Adv. Mater.* **2018**, *30*, 1704303.
[5] T. W. Tseng, T. T. Luo, S. H. Liao, K. H. Lu, K. L. Lu, *Angew. Chem. Int. Ed.* **2016**, *55*, 8343.
[6] S. Furukawa, J. Reboul, S. Diring, K. Sumida, S. Kitagawa, *Chem. Soc. Rev.* **2014**, *43*, 5700.
[7] A. Pathak, J. W. Shen, M. Usman, L. F. Wei, S. Mendiratta, Y. S. Chang, B. Sainbileg, C. M. Ngue, R. S. Chen, M. Hayashi, T. T. Luo, F. R. Chen, K. H. Chen, T. W. Tseng, L. C. Chen, K. L. Lu, *Nat. Commun.* **2019**, *10*, 1721.
[8] X. Xiao, L. Zou, H. Pang, Q. Xu, *Chem. Soc. Rev.* **2020**, *49*, 301.
[9] Q. Wang, D. Astruc, *Chem. Rev.* **2020**, *120*, 1438.
[10] D. E. Jaramillo, D. A. Reed, H. Z. H. Jiang, J. Oktawiec, M. W. Mara, A. C. Forse, D. J. Lussier, R. A. Murphy, M. Cunningham, V. Colombo, D. K. Shuh, J. A. Reimer, J. R. Long, *Nat. Mater.* **2020**, *19*, 517.
[11] S. Mendiratta, M. Usman, K. L. Lu, *Coord. Chem. Rev.* **2018**, *360*, 77.
[12] W. Cai, J. Wang, C. Chu, W. Chen, C. Wu, G. Liu, *Adv. Sci.* **2019**, *6*, 1801526.
[13] V. Stavila, A. A. Talin, M. D. Allendorf, *Chem. Soc. Rev.* **2014**, *43*, 5994.
[14] M. H. Yap, K. L. Fow, G. Z. Chen, *Green Energy Environ.* **2017**, *2*, 218.
[15] Y. Ye, W. Guo, L. Wang, Z. Li, Z. Song, J. Chen, Z. Zhang, S. Xiang, B. Chen, *J. Am. Chem. Soc.* **2017**, *139*, 15604.
[16] C. Zhou, L. Longley, A. Krajnc, G. J. Smales, A. Qiao, I. Erucar, C. M. Doherty, A. W. Thornton, A. J. Hill, C. W. Ashling, O. T. Qazvini, S. J. Lee, P. A. Chater, N. J. Terrill, A. J. Smith, Y. Yue, G. Mali, D. A. Keen, S. G. Telfer, T. D. Bennett, *Nat. Commun.* **2018**, *9*, 5042.
[17] C.-C. Wang, S.-Y. Ke, Y.-F. Hsieh, S.-T. Huang, T.-H. Wang, G.-H. Lee, Y.-C. Chuang, *J. Chin. Chem. Soc.* **2019**, *66*, 1031.
[18] K. Tan, N. Nijem, Y. Gao, S. Zuluag, J. Li, T. Thonhauser, Y. J. Chabal, *CrstEngComm* **2015**, *17*, 247.

[19] M. I. Gonzalez, J. A. Mason, E. D. Bloch, S. J. Teat, K. J. Gagnon, G. Y. Morrison, W. L. Queen, J. R. Long, *Chem. Sci.* **2017**, *8*, 4387.
[20] C. A. Trickett, A. Helal, B. A. Al-Maythalony, Z. H. Yamani, K. E. Cordova, O. M. Yaghi, *Nat. Rev. Mater.* **2017**, *2*, 17045.
[21] T. W. Tseng, L. W. Lee, T. T. Luo, P. H. Chien, Y. H. Liu, S. L. Lee, C. M. Wang, K. L. Lu, *Dalton Trans.* **2017**, *46*, 14728.
[22] C.-H. Lee, H.-Y. Huang, Y.-H. Liu, T.-T. Luo, G.-H. Lee, S.-M. Peng, J.-C. Jiang, I. Chao, K.-L. Lu, *Inorg. Chem.* **2013**, *52*, 3962.
[23] C.-H. Lee, H.-Y. Huang, J.-J. Lee, C.-Y. Huang, Y.-C. Kao, G.-H. Lee, S.-M. Peng, J.-C. Jiang, I. Chao, K.-L. Lu, *ChemistrySelect* **2016**, *1*, 2923.
[24] T.-R. Lin, C.-H. Lee, Y.-C. Lan, S. Mendiratta, L.-L. Lai, J.-Y. Wu, K.-M. Chi, K.-L. Lu, *Polymers* **2018**, *10*, 1398.
[25] S.-H. Lin, C.-I. Yang, T.-S. Kuo, M.-H. Chiang, K.-C. Hsu, K.-L. Lu, *Dalton Trans.* **2012**, *41*, 1448.
[26] C.-H. Ke, G.-R. Lin, B.-C. Kuo, H. M. Lee, *Cryst. Growth Des.* **2012**, *12*, 3758.
[27] T.-Y. Ho, S.-M. Huang, J.-Y. Wu, K.-C. Hsu, K.-L. Lu, *Cryst. Growth Des.* **2015**, *15*, 4266.
[28] X.-K. Yang, J.-D. Chen, *CrstEngComm* **2019**, *21*, 7437.
[29] F.-K. Shieh, S.-C. Wang, C.-I. Yen, C.-C. Wu, S. Dutta, L.-Y. Chou, J. V. Morabito, P. Hu, M.-H. Hsu, K. C.-W. Wu, C.-K. Tsung, *J. Am. Chem. Soc.* **2015**, *137*, 4276.
[30] M. J. Rosseinsky, *Micropor. Mesopor. Mater.* **2004**, *73*, 15.
[31] Z.-J. Lin, J. Lu, M. Hong, R. Cao, *Chem. Soc. Rev.* **2014**, *43*, 5867.
[32] S.-S. Chen, *CrstEngComm* **2016**, *18*, 6543.
[33] A. G. Lvov, M. Mörtel, A. V. Yadykov, F. W. Heinemann, V. Z. Shirinian, M. M. Khusniyarov, *Beilstein J. Org. Chem.* **2019**, *15*, 2428.
[34] J.-B. Lin, J.-P. Zhang, X.-M. Chen, *J. Am. Chem. Soc.* **2010**, *132*, 6654.
[35] S. Bureekaew, H. Sato, R. Matsuda, Y. Kubota, R. Hirose, J. Kim, K. Kato, M. Takata, S. Kitagawa, *Angew. Chem. Int. Ed.* **2010**, *49*, 7660.
[36] S. Sen, S. Neogi, A. Aijaz, Q. Xu, P. K. C. Bharadwaj, *Inorg. Chem.* **2014**, *53*, 7591.
[37] X.-L. Hu, F.-H. Liu, H.-N. Wang, C. Qin, C.-Y. Sun, Z.-M. Su, F.-C. Liu, *J. Mater. Chem. A* **2014**, *2*, 14827.
[38] D.-M. Chen, X.-P. Zhang, W. Shi, P. Cheng, *Cryst. Growth Des.* **2014**, *14*, 6261.
[39] X.-L. Hu, Q.-H. Gong, R.-L. Zhong, X.-L. Wang, C. Qin, H. Wang, J. Li, K.-Z. Shao, Z.-M. Su, *Chem. A Eur. J.* **2015**, *21*, 7238.
[40] A. Schneemann, P. Vervoorts, I. Hante, M. Tu, S. Wannapaiboon, C. Sternemann, M. Paulus, D. C. F. Wieland, S. Henke, R. A. Fischer, *Chem. Mater.* **2018**, *30*, 1667.
[41] L.-W. Lee, T.-T. Luo, S.-H. Lo, G.-H. Lee, S.-M. Peng, Y.-H. Liu, S.-L. Lee, K.-L. Lu, *CrstEngComm* **2015**, *17*, 6320.
[42] Y.-H. Lu, H.-T. Chen, *J. Chin. Chem. Soc.* **2016**, *63*, 459.
[43] A. Dey, S. Bera, K. Biradha, *Cryst. Growth Des.* **2015**, *15*, 318.
[44] Z. Otwinowski, W. Minor, in *Macromolecular Crystallography, Part A*, Vol. 276 (Eds: C. W. Carter Jr., R. M. Sweet), Academic Press, New York, NY **1997**, p. 307.
[45] Bruker, *SADABS*, Bruker AXS Inc, Madison, WI **2000**.
[46] G. M. Sheldrick, *Acta Crystallogr. A Found. Crystallogr.* **2008**, *64*, 112.

SUPPORTING INFORMATION

Additional supporting information may be found online in the Supporting Information section at the end of this article.

How to cite this article: Wu H-W, Lee L-W, Thanasekaran P, et al. Weak interactions in imidazole-containing zinc(II)-based metal–organic frameworks. *J Chin Chem Soc*. 2020;1–7. https://doi.org/10.1002/jccs.202000106